RESEARCH PAPER

Optimized Phospho-Aspirin Derivatives Target EGFR T790M/L858R and Suppress Oncogenic Signaling in Resistant NSCLC: In Vitro Mechanistic and In Vivo Xenograft Validation

Madhuri Rudraraju[1,2], Vasudha Bakshi[1*]

[1] Department of Pharmacology, School of Pharmacy, Anurag University, Ghatkesar, Hyderabad-500088, India.

[2] Centre for Pharmaceutical Sciences (CPS), Jawaharlal Nehru Technology University (JNTU), Hyderabad-500072, India.

[*] **Corresponding Author:** Dr. Vasudha Bakshi, Professor, and Dean, Dept. of Pharmacology, School of Pharmacy, Anurag University, Ghatkesar, Hyderabad-500088, Telangana, India.

Email: vasudhapharma.anurag@gmail.com

1st Author Email: madhuri8008@gmail.com

ABSTRACT

The emergence of resistance to epidermal growth factor receptor (EGFR) tyrosine kinase inhibitors, particularly due to the T790M mutation, remains a major challenge in the treatment of non-small-cell lung cancer (NSCLC). In this study, we report the design, optimization, and comprehensive biological evaluation of novel phospho-aspirin derivatives that target EGFR T790M/L858R-driven oncogenic signaling. The objective of this study was to identify potent, mutation-selective inhibitors capable of overcoming resistance and demonstrating translational therapeutic potential. Lead optimization was performed through integrated in silico screening, ADME profiling, and biological validation, which led to the identification of PA03 and PA12. In vitro cytotoxicity studies across NSCLC cell lines (A549, H3255, PC9, and H1975) revealed that PA12 exhibited superior potency (IC_{50}: 0.71–0.93 nM), outperforming PA03 and demonstrating comparable or enhanced efficacy relative to osimertinib. Selectivity index analysis confirmed the strong tumor specificity of PA12, with minimal toxicity toward normal cells. Enzymatic kinase inhibition assays demonstrated potent and mutation-selective inhibition of EGFR T790M/L858R (IC_{50}: 22.4 nM), surpassing that of osimertinib. Mechanistic studies using western blot analysis revealed significant suppression of EGFR phosphorylation and downstream PI3K/AKT and MAPK/ERK pathways, accompanied by increased Bax expression and decreased Bcl-2 levels. Caspase-3/7 and caspase-9 assays further confirmed the robust activation of intrinsic apoptosis. In vivo evaluation using an H1975 xenograft model demonstrated significant tumor growth inhibition by PA12 (61.8%), exceeding that of osimertinib, with no observable systemic toxicity, as evidenced by stable body weight and normal biochemical parameters. Collectively, these findings establish PA12 as a potent, mutation-selective EGFR inhibitor with superior efficacy in resistant NSCLC, highlighting its potential as a promising next-generation therapeutic candidate for NSCLC.

Keywords: Phospho-aspirin derivatives, EGFR T790M/L858R, NSCLC, targeted therapy, kinase inhibition, apoptosis, xenograft model, drug resistance.

How to cite this article: Rudraraju M, Bakshi V. Optimized Phospho-Aspirin Derivatives Target EGFR T790M/L858R and Suppress Oncogenic Signaling in Resistant NSCLC: in vitro Mechanistic and in vivo Xenograft Validation. Int J Drug Deliv Technol. 2026;16(35s): 1174-1186. DOI: 10.25258/ijddt.16.35s.130

Source of support: Nil.

Conflict of interest: None

INTRODUCTION

Non-small cell lung cancer (NSCLC) accounts for approximately 85% of all lung cancer cases and remains a leading cause of cancer-related mortality worldwide despite advances in targeted therapies and immunotherapy (Siegel et al., 2023; Herbst et al., 2018). Among the key oncogenic drivers of NSCLC, aberrations in the epidermal growth factor receptor (EGFR) gene play a pivotal role in tumor initiation and progression. Activating mutations, such as exon 19 deletions and the L858R point mutation, lead to the constitutive activation of EGFR-mediated signaling pathways, including PI3K/Akt and MAPK/ERK, thereby promoting uncontrolled cell proliferation, survival, and metastasis (Yarden and Sliwkowski, 2001; Sharma et al., 2007). The development of EGFR tyrosine kinase inhibitors (TKIs), including first-generation agents such as gefitinib and erlotinib and second-generation inhibitors such as afatinib, has significantly improved clinical

outcomes in patients with EGFR mutations (Mok et al., 2009; Sequist et al., 2013). However, the therapeutic benefits of these agents are often transient because of the emergence of acquired resistance. The T790M gatekeeper mutation, present in over 50% of resistant cases, enhances ATP affinity and sterically interferes with inhibitor binding, thereby diminishing the drug efficacy (Pao et al., 2005; Yun et al., 2008). Although third-generation TKIs, such as osimertinib, have been developed to target T790M-positive tumors, resistance inevitably develops through additional mechanisms, including secondary mutations, HER2 amplification, and activation of bypass signaling pathways (Cross et al., 2014; Leonetti et al., 2019). These limitations underscore the urgent need for novel therapeutic strategies that can effectively target resistant EGFR mutants and associated oncogenic signaling networks.

In recent years, drug repurposing has emerged as a promising strategy for accelerating the development of novel anticancer agents by leveraging existing pharmacological scaffolds with known safety profiles (Pushpakom et al., 2019). Aspirin (acetylsalicylic acid), a widely used nonsteroidal anti-inflammatory drug, has demonstrated chemopreventive and anticancer properties in multiple cancer types, including lung cancer (Cuzick et al., 2015). However, its clinical application in oncology is limited by its poor selectivity and systemic toxicity. To overcome these limitations, phospho-aspirin derivatives have been developed by conjugating phosphate or phosphonate moieties to aspirin scaffolds. These modifications enhance aqueous solubility, improve pharmacokinetic properties, and facilitate tumor-selective uptake, thereby augmenting anticancer efficacy and minimizing toxicity (Zhao et al., 2018; Hua et al., 2020). From a medicinal chemistry perspective, rational modification of the aspirin scaffold provides an opportunity to design multifunctional molecules that can target key oncogenic pathways. In particular, the incorporation of phosphate groups enables ATP-mimetic interactions within kinase domains, whereas hydrophobic linkers enhance binding within the EGFR ATP-binding pocket. These structural features may enable effective inhibition of EGFR T790M/L858R mutants and overcome steric resistance mechanisms. Despite these advancements, a critical gap remains in the comprehensive mechanistic and in vivo validation of optimized phospho-aspirin derivatives targeting resistant EGFR-driven NSCLC. Based on this rationale, we hypothesized that optimized phospho-aspirin derivatives could selectively inhibit EGFR T790M/L858R kinase activity, suppress downstream oncogenic signaling pathways, and induce apoptosis in NSCLC models resistant to treatment. Furthermore, these effects may translate into significant antitumor efficacy in vivo studies. Accordingly, the present study aimed to systematically preclinically evaluate the optimized phospho-aspirin derivatives using integrated in vitro and in vivo approaches.

In this study, selected lead compounds were first evaluated for cytotoxic potency and selectivity in EGFR-mutant NSCLC cell lines, followed by target-level validation using the kinase inhibition assays. Mechanistic investigations were conducted to assess the impact on receptor tyrosine kinases and downstream signaling pathways, including the PI3K/Akt cascade, along with apoptosis-related proteins such as Bax, Bcl-2, and cytochrome c. Apoptosis induction was further confirmed using caspase-3/7 and caspase-9 assays. Finally, the antitumor efficacy of the optimized lead compound was evaluated in an H1975 xenograft mouse model to establish *its in vivo* therapeutic potential. Collectively, this study provides comprehensive mechanistic and preclinical validation of optimized phospho-aspirin derivatives as promising therapeutic candidates for overcoming EGFR mutation-driven resistance in NSCLC, thereby offering a potential avenue for the development of next-generation targeted anticancer agents.

MATERIALS AND METHODS

Validation of *in vitro* cytotoxic potency

The antiproliferative activities of the optimized phosphoaspirins, **PA03** and **PA12**, were evaluated in NSCLC cell lines H1975, H3255, PC9, and A549 using the MTT assay. Cells were seeded in 96-well plates at a density of 8×10^3 cells/well and incubated for 24 h at 37 °C and 5% CO_2. The medium was then replaced with fresh medium containing test compounds at concentrations of 0–10 μM (0, 0.156, 0.312, 0.625, 1.25, 2.5, 5, and 10 μM). The final DMSO concentration was maintained at ≤0.1% v/v. Gefitinib and osimertinib were used as reference controls along with untreated and vehicle controls. Following 48 h of treatment, 20 μL of MTT solution (5 mg/mL) was added and incubated for 3-4 h. The medium was removed, and the formazan crystals were dissolved in 150 μL DMSO. Absorbance was measured at 570 nm. Cell viability was expressed

relative to that of the control, and IC_{50} values were determined using nonlinear regression analysis.

Selectivity index (SI) determination

The selectivity of **PA03** and **PA12** was assessed in NSCLC cell lines H1975, H3255, PC9, and A549, with BEAS-2B as the normal epithelial control, using the MTT assay under the same conditions. Cells were seeded at 8 × 10^3 cells/well in 96-well plates and incubated for 24 h (37 °C, 5% CO_2). Subsequently, the cells were treated with **PA03** and **PA12** (0–10 μM) for 48 h, maintaining DMSO ≤0.1% v/v, with untreated and vehicle controls included. After treatment, 20 μL of MTT solution (5 mg/mL) was added and incubated for 3–4 h. Formazan crystals were dissolved in 150 μL DMSO, and the absorbance was measured at 570 nm. Cell viability was calculated relative to that of the control, and IC_{50} values were obtained using nonlinear regression analysis. The SI was calculated for each cancer cell line using the following formula: Higher SI values indicate greater tumor selectivity and reduced toxicity toward normal cells.

$$SI = \frac{IC_{50,\ BEAS-2B}}{IC_{50,\ cancer\ cell\ line}}$$

EGFR kinase inhibition assay (ADP-Glo luminescence assay)

The inhibitory activities of **PA03** and **PA12** against EGFR kinase variants (wild-type, L858R, T790M, and T790M/L858R) were evaluated using a luminescence-based ADP-Glo kinase assay (Promega). Reactions were performed in white 96-well plates (25 μL total volume) containing kinase buffer (40 mM Tris-HCl, pH 7.5; 20 mM $MgCl_2$; 0.1 mg/mL BSA; 50 μM DTT), EGFR enzyme (10–20 ng), and poly(Glu,Tyr) (4:1) substrates (0.2 mg/mL). Test compounds were added at 5–100 nM (5, 10, 20, 40, 60, 80, and 100 nM) with dimethyl sulfoxide (DMSO) ≤0.1% v/v. Gefitinib and osimertinib served as reference inhibitors, and enzyme and blank controls were included. The reaction was initiated with ATP (50 μM) and incubated at 30 °C for 40 min. The reaction was terminated by adding 25 μL ADP-Glo reagent and incubating for 40 min, followed by the addition of 50 μL kinase detection reagent and incubation for 30 min. Luminescence was measured using a microplate luminometer. The % inhibition was calculated relative to the enzyme control, and IC_{50} values were determined using nonlinear regression analysis.

Westernblot analysis

Western blot analysis was performed to evaluate mutation-specific EGFR expression, RTK signaling suppression, downstream pathway modulation, and apoptosis induction following treatment with **PA03** and **PA12**. Based on the EGFR genotype, H1975 cells were used to evaluate EGFR L858R/T790M dual-mutant signaling, H3255 cells for EGFR L858R, PC9 cells for EGFR exon 19 deletion/T790M-associated signaling, and A549 cells for wild-type EGFR assessment. Cells were treated with **PA03**, **PA12**, and osimertinib at the IC_{50} concentrations for 24 h. After treatment, the cells were washed with ice-cold PBS and lysed using RIPA buffer containing protease and phosphatase inhibitors. Lysates were centrifuged at 12,000 rpm for 15 min at 4 °C, and the protein concentration was estimated using the BCA assay. Equal amounts of protein were separated by SDS-PAGE and transferred onto PVDF membranes. The membranes were blocked with 5% BSA or non-fat skimmed milk in TBST for 1 h and incubated overnight at 4 °C with primary antibodies against total EGFR, p-EGFR (A549), EGFR L858R (Both H1975 and H3255), EGFR T790M (both H1975 and PC9), PI3K, AKT, p-ERK, Bax, Bcl-2 (from mutant 3 cell lines), and β-actin, which was used as a loading control. Following washing, the membranes were incubated with the appropriate HRP-conjugated secondary antibodies for 1 h at room temperature. The bands were visualized using an ECL detection system and imaged using a gel documentation system. Densitometric analysis was performed using ImageJ software, normalized to β-actin, and expressed relative to the untreated control. Mutation-specific EGFR blots were interpreted according to the corresponding cell line genotype, and PI3K/AKT, ERK, and apoptosis-related proteins were assessed to determine downstream pathway suppression and mitochondrial apoptosis activation.

Caspase-3/7 and caspase-9 activity assays

Caspase-3/7 and caspase-9 activities were evaluated to confirm the induction of apoptosis by **PA03** and **PA12** in NSCLC cells. Briefly, the cells were seeded in sterile 96-well plates and allowed to attach overnight under standard culture conditions. Cells were then treated with **PA03, PA12,** and osimertinib at the IC_{50} for 24 h**,** and untreated and vehicle-treated cells served as controls. After treatment, caspase assay reagents specific for caspase-3/7 and caspase-9 were added separately to the respective wells according to the manufacturer's instructions and incubated at room temperature in the dark. For spectrophotometric estimation, the cleavage of chromogenic substrates was measured using a

microplate reader at the recommended wavelength of 405 nm**.** The absorbance intensity was proportional to the caspase enzymatic activity. Caspase activity was calculated relative to that of the untreated control cells and expressed as fold change**.** Increased caspase-3/7 activity indicated the activation of executioner caspases, whereas elevated caspase-9 activity confirmed the involvement of the intrinsic mitochondrial apoptotic pathway.

***In vivo* antitumor evaluation in H1975 xenograft model**

Female athymic nude mice (5–6 weeks old, 18–22 g) were used for in vivo evaluation following approval from the Institutional Animal Ethics Committee (IAEC) in accordance with CPCSEA guidelines (File No. PGPLS/77/IAEC/0039/2024). Animals were acclimatized for one week and maintained under controlled conditions (22 ± 2 °C, 50–60% humidity, 12 h light/dark cycle) with free access to a standard diet and water. General health, behavior, and signs of distress were monitored during the study. A resistant NSCLC xenograft model was established using H1975 (EGFR L858R/T790M) cells. Cells in the exponential phase were harvested, washed with phosphate-buffered saline (PBS), and resuspended in a serum-free medium. The cell suspension was mixed with Matrigel (1:1), and 5×10^6 cells in 100 µL were injected subcutaneously into the right flank of each mouse. Tumor growth was monitored, and treatment was initiated when the tumor volume reached approximately 100–120 mm^3. Animals were randomly divided into groups (n = 6 per group): Group I (vehicle control), Group II (**PA12**, at a dose of 5 mg/kg bw), and Group III (osimertinib, positive control at 5 mg/kg bw). All treatments were administered once daily via oral gavage for 28 days, with the formulations freshly prepared in 0.5% carboxymethylcellulose. Animals were observed throughout the study for signs of toxicity and behavioral changes. Tumor dimensions were measured twice weekly using digital calipers, and the tumor volume was calculated using the following formula:

$$\text{Tumor volume } (mm^3) = \frac{\text{Length} \times \text{Width}^2}{2}$$

Body weight was recorded periodically to assess the tolerability of the treatment. At the end of the study, the animals were euthanized, and the tumors were excised, washed, and weighed. Tumor growth inhibition (TGI%) was calculated relative to that of the control group. For safety assessment, the animals were monitored for physiological and behavioral changes during treatment. At the end of the study, blood samples were collected under anesthesia via appropriate routes, allowed to clot, and centrifuged to obtain serum. Serum samples were analyzed for biochemical parameters, including AST, ALT, urea, and creatinine levels, using standard diagnostic kits.

Statistical analysis

All in vitro and in vivo experiments were performed in triplicate or with a minimum of six animals per group, and the data are expressed as the mean ± standard deviation (SD). For in vitro studies, including cytotoxicity (MTT), kinase inhibition, western blot densitometry, and caspase activity assays, statistical comparisons between multiple groups were conducted using one-way analysis of variance (ANOVA) followed by Tukey's post hoc test to determine intergroup significance. Dose–response curves and IC_{50} values were calculated using nonlinear regression analysis in GraphPad Prism. For in vivo studies, tumor volume progression and body weight data were analyzed using two-way ANOVA, whereas endpoint parameters such as tumor weight and biochemical markers were evaluated using one-way ANOVA, followed by appropriate post hoc comparisons. Statistical significance was set at $p < 0.05$. Graphical representations were generated using GraphPad Prism, and all statistical analyses were performed to ensure the reliability, reproducibility, and validity of the experimental findings.

RESULTS AND DISCUSSION

Lead Selection

The final lead selection was performed through an integrated analysis of in silico screening, cytotoxic evaluation, and mechanistic validation of the synthesized phospho-aspirin derivatives(Madhuri Rudraraju et al., 2022). Initially, ADME-based prioritization identified PA-01 to PA-13 as drug-like candidates with favorable physicochemical properties and zero Lipinski rule violations, ensuring their suitability for further biological evaluation (Rudraraju et al., 2022). Subsequent in vitro screening of EGFR-mutant NSCLC cell lines revealed that PAh3 and PAh12 exhibited superior antiproliferative activity, with consistently low micromolar IC_{50} values across both drug-sensitive and resistant models, including H1975 (EGFR T790M/L858R) (Madhuri Rudraraju et al., 2022). Importantly, these leads demonstrated enhanced efficacy compared to gefitinib, particularly in T790M-driven resistant cells, highlighting their

ability to overcome classical EGFR-TKI resistance. Morphological and apoptosis-based assays further confirmed the pronounced cytotoxic and pro-apoptotic effects of h3 and h12, establishing their biological significance. Additionally, kinase inhibition studies showed potent suppression of EGFR T790M/L858R activity, with h3 exhibiting potency comparable to that of osimertinib (Rudraraju et al., 2022). Collectively, the convergence of drug-likeness, broad-spectrum cytotoxicity, and strong target-level inhibition led to the selection of h3 and h12 as optimized lead candidates for further mechanistic and in vivo validation studies.

Reassessment of *in vitro* cytotoxic potency of PA03 and PA12

The antiproliferative activities of the optimized phosphoaspirin derivatives, **PA03** and **PA12**, were systematically evaluated in NSCLC cell lines with diverse EGFR mutational backgrounds, including A549 (wild-type), H3255 (L858R), PC9 (exon 19 deletion), and H1975 (L858R/T790M). As summarized in Table 1, **PA12** exhibited strong and consistent cytotoxic activity across all tested cell lines, with IC_{50} values ranging from 0.71 to 0.93 µM. Notably, **PA12** demonstrated the highest potency in the H1975 resistant cell line (IC_{50} = 0.71 nM), indicating its effectiveness against EGFR T790M-mediated resistance. In comparison, osimertinib, a third-generation EGFR inhibitor, showed comparable cytotoxicity with IC_{50} values between 0.78 and 0.91 µM, validating the assay conditions and confirming its efficacy against mutant EGFR forms. While **PA12** exhibited slightly higher potency than osimertinib in H3255 and H1975 cells, its activity was comparable in PC9 cells and slightly lower in A549 cells, suggesting a mutation-dependent response. In contrast, **PA03** exhibited moderate cytotoxic activity across all cell lines, with IC_{50} values ranging from 1.38 to 1.52 µM, indicating that the potency observed in PA12 was significantly enhanced by structural optimization. As expected, gefitinib demonstrated markedly reduced activity in EGFR-mutant and resistant models, particularly in H3255, PC9, and H1975 cells (IC_{50} = 5.42–7.96 µM), consistent with the established resistance mechanisms associated with T790M and other mutations.

The dose–response curves presented in Figure 1a and 1b further corroborate these findings, showing a clear concentration-dependent decrease in cell viability for both compounds. **PA12** exhibited a steeper inhibition profile than **PA03**, particularly at lower concentrations, highlighting its superior pharmacological performance. The pronounced cytotoxic effect of **PA12** in resistant H1975 cells further underscores its ability to overcome resistance-associated signaling pathways. These findings are consistent with those of a previous study by Rudraraju et al. (2022), in which phosphoaspirin derivatives demonstrated potent antiproliferative activity in EGFR-mutant NSCLC models. The improved efficacy of **PA12** relative to **PA03** reinforces the critical role of structural optimization in enhancing target engagement and overcoming drug resistance. Gefitinib showed reduced activity in EGFR-resistant cells, whereas osimertinib retained potent efficacy, indicating superior mutation-targeted inhibition. Collectively, these results demonstrate that **PA12** is a promising lead compound with potent and broad-spectrum activity across both sensitive and resistant NSCLC models, exhibiting comparable or improved efficacy relative to osimertinib and significantly outperforming first-generation EGFR inhibitors such as gefitinib.

Table. 1 IC_{50} values of optimized phospshoaspirins **PA03** and **PA12** in NSCLC cell lines

Treatment	A549 (µM)	H3255 (µM)	PC9 (µM)	H1975 (µM)
PA12	0.93 ± 0.05	0.78 ± 0.06	0.83 ± 0.07	0.71 ± 0.05
Osimertinib	0.82 ± 0.06	0.91 ± 0.07	0.78 ± 0.05	0.86 ± 0.06
PA03	1.38 ± 0.12	1.46 ± 0.14	1.52 ± 0.15	1.41 ± 0.13
Gefitinib	1.62 ± 0.15	7.96 ± 0.41	5.42 ± 0.33	5.73 ± 0.36

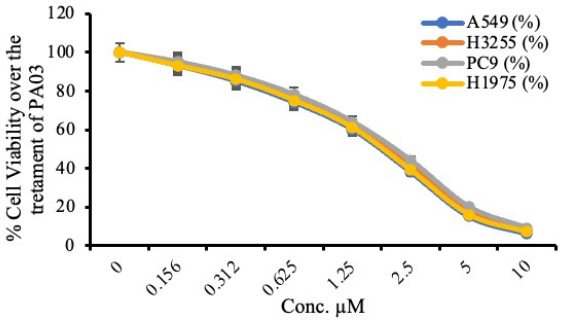

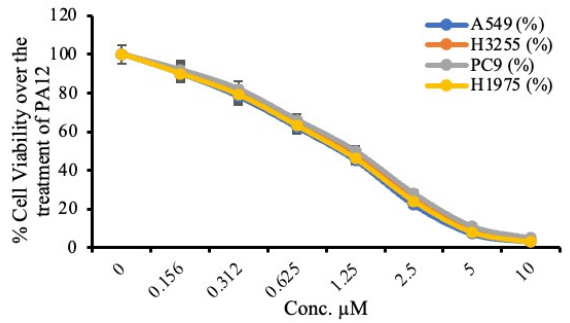

Figure 1. *In vitro* cytotoxicity of the optimized phosphoaspirin derivatives in NSCLC cell lines (1a). Dose–response curves of **PA03** in A549, H3255, PC9, and H1975 cells after 48 h of treatment, showing a concentration-dependent reduction in cell viability, including in EGFR T790M mutant H1975 cells. **(**1b). The dose-response curves of **PA12** in A549, H3255, PC9, and H1975 cells after 48 h of treatment demonstrated significant concentration-dependent cytotoxicity across all cell lines. Data are expressed as mean ± SD (n = 3)**;** one-way ANOVA with Tukey's post hoc test was applied (*p < 0.05 vs. control).

Selectivity index

The tumor selectivity of the optimized phosphoaspirin derivatives, **PA03** and **PA12**, was evaluated by calculating the selectivity index (SI) of NSCLC cell lines relative to normal bronchial epithelial cells (BEAS-2B). As presented in Table 2, **PA12** demonstrated the highest selectivity across all tested cell lines, with SI values ranging from 12.46 ± 0.98 to 14.47 ± 1.12, indicating strong preferential cytotoxicity toward cancer cells. Notably, **PA12** exhibited a high SI in the resistant H1975 (L858R/T790M) model (13.86 ± 1.09), confirming its ability to selectively target resistant tumor cells while sparing normal epithelial cells. In comparison, osimertinib showed moderate selectivity, with SI values between 7.05 ± 0.55 and 8.23 ± 0.64, which is consistent with its known efficacy against mutant EGFR. **PA03** displayed comparatively lower selectivity (SI ≈ 5.34–5.88), suggesting that further structural optimization of **PA12** significantly improved its tumor specificity. As expected, gefitinib exhibited poor selectivity in EGFR-mutant models, particularly in H3255, PC9, and H1975 cells (SI ≈ 1.30–1.91), reflecting its reduced efficacy and lack of discrimination between cancerous and normal cells under resistant conditions. The consistently higher SI values of **PA12** across all NSCLC models, including both mutant and wild-type cells, highlight its improved therapeutic window and reduced cytotoxicity toward normal bronchial epithelial cells. These findings strongly support the superiority of **PA12** over **PA03** and first-generation EGFR inhibitors and demonstrate comparable or enhanced selectivity relative to osimertinib. Collectively, the selectivity analysis confirmed that **PA12** possesses enhanced tumor-targeting capability with minimal off-target toxicity, thereby reinforcing its potential as a promising lead candidate for further mechanistic and in vivo validation in EGFR-driven resistant NSCLC.

Table 2. SI of optimized phosphoaspirin derivatives across NSCLC cell lines

Treatment	BEAS-2B IC_{50} (µM)	A549 SI	H3255 SI	PC9 SI	H1975 SI
PA12	9.84 ± 0.72	14.47 ± 1.12	13.29 ± 1.05	12.46 ± 0.98	**13.86 ± 1.09**
Osimertinib	6.42 ± 0.48	7.83 ± 0.62	7.05 ± 0.55	8.23 ± 0.64	7.46 ± 0.58
PA03	8.12 ± 0.65	5.88 ± 0.46	5.56 ± 0.44	5.34 ± 0.42	5.76 ± 0.45
Gefitinib	10.35 ± 0.83	6.39 ± 0.51	1.30 ± 0.10	1.91 ± 0.15	1.81 ± 0.14

Target-level kinase inhibition Studies

The direct inhibitory potential of the optimized phosphoaspirin derivatives was evaluated against multiple EGFR variants, including wild-type, L858R, T790M, and dual mutant T790M/L858R, using a luminescence-based ADP-Glo kinase assay. The results demonstrated a clear mutation-guided inhibition pattern, with maximal activity observed against the dual-mutant EGFR (T790M/L858R), followed by single mutants, and comparatively reduced activity against the wild-type EGFR (Table 3; Figure 2a–d). Among the tested compounds, **PA12** consistently exhibited the highest inhibitory potency across all EGFR variants, with an IC_{50} value of 22.4 ± 1.9 nM against the dual mutant, outperforming the standard drug osimertinib (27.3 ± 2.2 nM). This superior activity was further reflected in the percentage inhibition data, where **PA12** achieved ~98.6% inhibition at 100 nM against the dual mutant, compared to ~94.8% for osimertinib at the same concentration level. These findings strongly indicate an enhanced binding affinity and effective targeting of resistance-associated EGFR conformations. In single mutant forms, **PA12** maintained high potency, with IC_{50} values of 44.3 ± 3.5

nM (L858R) and 40.7 ± 3.2 nM (T790M), demonstrating broad-spectrum inhibition across clinically relevant EGFR mutations. The corresponding inhibition profiles showed a consistent concentration-dependent increase, with **PA12** achieving >90% inhibition at higher concentrations, thereby confirming its strong enzymatic efficacy. In contrast, **PA03** exhibited moderate inhibitory activity, with higher IC_{50} values (74.5 ± 5.9 nM for the dual mutant) and reduced percentage inhibition across all variants, highlighting the impact of structural optimization on **PA12**. As expected, gefitinib showed significantly reduced activity against T790M-containing variants, particularly dual mutants, confirming its known limitations in resistance settings. Although gefitinib moderately inhibited L858R and wild-type EGFR, its overall performance was inferior to that of **PA12** and osimertinib. Importantly, all compounds demonstrated comparatively lower inhibition against wild-type EGFR, with **PA12** showing an IC_{50} of 72.8 ± 5.6 nM, indicating a degree of mutation selectivity. This selective inhibition profile is desirable for minimizing off-target toxicity while maintaining efficacy against mutant EGFR-driven tumors. The dose–response curves (Figure 2a–d) further validated these observations, showing a steeper inhibition profile for **PA12** across all variants, particularly in the dual mutant, followed by osimertinib, **PA03**, and gefitinib. The consistent trend across all datasets confirmed the superiority of **PA12** as a lead compound with enhanced potency and mutation-selective inhibition properties. Collectively, these findings establish that **PA12** effectively targets EGFR T790M/L858R and other mutant forms with high potency while maintaining reduced activity toward wild-type EGFR, demonstrating a favorable selectivity profile.

Table 3. EGFR kinase inhibition IC_{50} (nM) of optimized compounds across EGFR variants

Treatment	EGFR (WT) IC_{50} (nM)	EGFR L858R IC_{50} (nM)	EGFR T790M IC_{50} (nM)	EGFR T790M/L858R IC_{50} (nM)
PA 12	72.8 ± 5.6	44.3 ± 3.5	40.7 ± 3.2	22.4 ± 1.9
Osimertinib	81.5 ± 6.2	52.6 ± 4.1	47.8 ± 3.7	27.3 ± 2.2
PA 3	118.6 ± 9.4	86.2 ± 6.8	93.4 ± 7.3	74.5 ± 5.9
Gefitinib	95.7 ± 7.5	63.8 ± 5.0	78.6 ± 6.2	60.9 ± 4.8

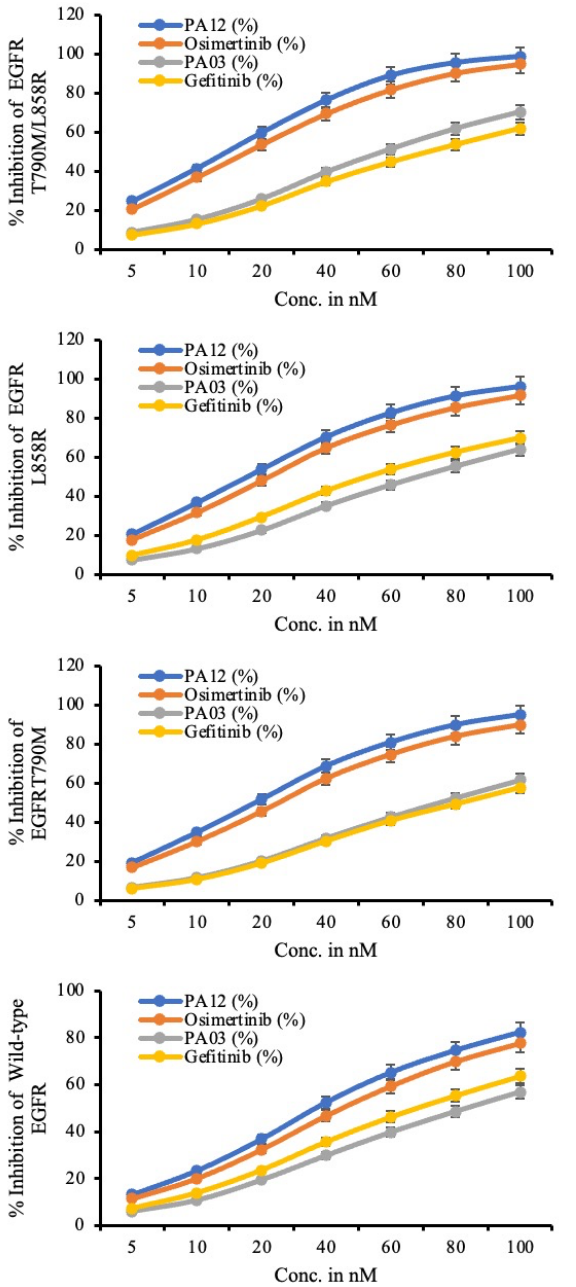

Figure 2. EGFR kinase inhibition profiles of the optimized phosphoaspirin derivatives; (2a) dose–response inhibition curves of **PA12**, **PA03**, osimertinib, and gefitinib against EGFR T790M/L858R dual mutants, showing superior inhibition by **PA12** across all concentrations. (2b) Concentration-dependent inhibition of EGFR L858R mutant, demonstrating the enhanced potency of **PA12**

compared to that of the standards and **PA03**. (2c) The inhibition profile against the EGFR T790M mutant indicated effective targeting of resistance-associated mutations, with **PA12** exhibiting the highest inhibitory activity. (2d) Inhibition curves for wild-type EGFR showed comparatively reduced activity across all compounds, with **PA12** exhibiting moderate inhibition. Statistical analysis: Data are presented as mean ± SD (n = 3). Statistical significance was evaluated using one-way ANOVA followed by Tukey's post hoc test, with *p < 0.05 considered significant compared to control.

Western blot analysis

Western blot analysis was performed to delineate the molecular effects of **PA03** and **PA12** on EGFR-driven oncogenic signaling and apoptosis in NSCLC models. The representative blots and corresponding densitometric analyses (Figure 3a–f) demonstrated a consistent and pronounced inhibitory effect following the activity trend **PA12** > osimertinib > **PA03**. As shown in Figure 3a and 3b, treatment with **PA12** resulted in marked suppression of total EGFR and phosphorylated EGFR (p-EGFR) in A549 cells, indicating effective inhibition of basal receptor activation. More importantly, mutation-specific analysis revealed significant downregulation of EGFR L858R (H1975 and H3255) and EGFR T790M (H1975 and PC9) upon **PA12** treatment, confirming its ability to target both activating and resistance-associated EGFR variants in NSCLC cells. The extent of suppression was consistently greater than that observed with **PA03** and slightly superior to that of osimertinib, highlighting the enhanced target engagement of **PA12**. Further mechanistic insights were obtained from downstream signaling analysis (Figure 3c and 3d). **PA12** substantially inhibited PI3K, AKT, and p-ERK expression in H1975, H3255, and PC9 cells, indicating effective blockade of both the PI3K/AKT survival pathway and the MAPK/ERK proliferative axis. In contrast, **PA03** exhibited moderate inhibition, and osimertinib exhibited intermediate effects. The pronounced suppression of p-ERK by **PA12** suggests an efficient disruption of mitogenic signaling cascades downstream of the mutant EGFR. Apoptotic protein profiling (Figure 3e and 3f) revealed a significant shift toward pro-apoptotic signaling following **PA12** treatment. Specifically, Bax expression was markedly upregulated, whereas Bcl-2 levels were substantially reduced across all mutant cell lines, indicating the activation of the intrinsic mitochondrial apoptotic pathway. These effects were more prominent with **PA12** than with **PA03** and were comparable to or exceeded those observed with osimertinib. Collectively, the Western blot findings provide strong mechanistic evidence that **PA12** exerts potent mutation-selective inhibition of EGFR signaling, effectively suppressing downstream oncogenic pathways and robustly inducing apoptosis in resistant NSCLC models. The superior performance of **PA12** across all evaluated parameters underscores its potential as an advanced therapeutic candidate capable of overcoming EGFR T790M/L858R-mediated resistance.

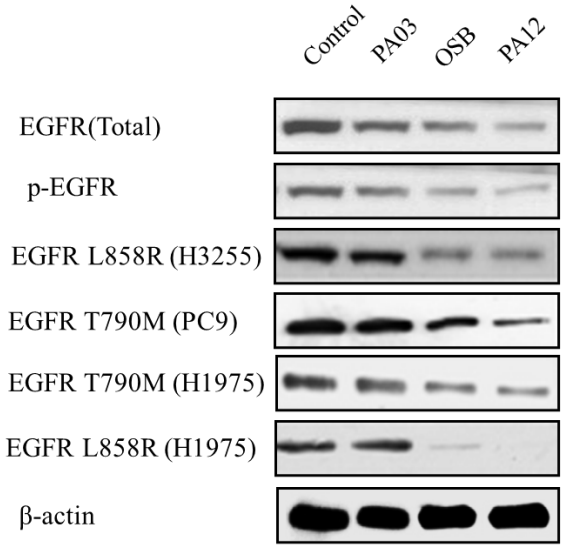

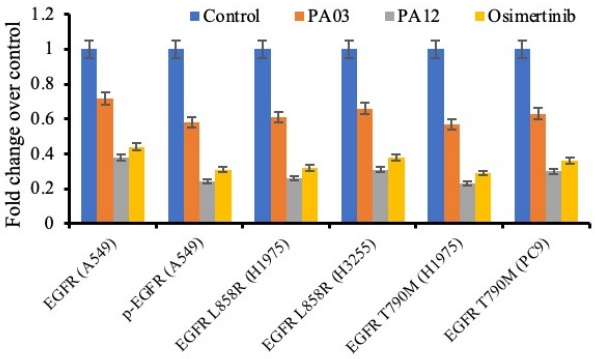

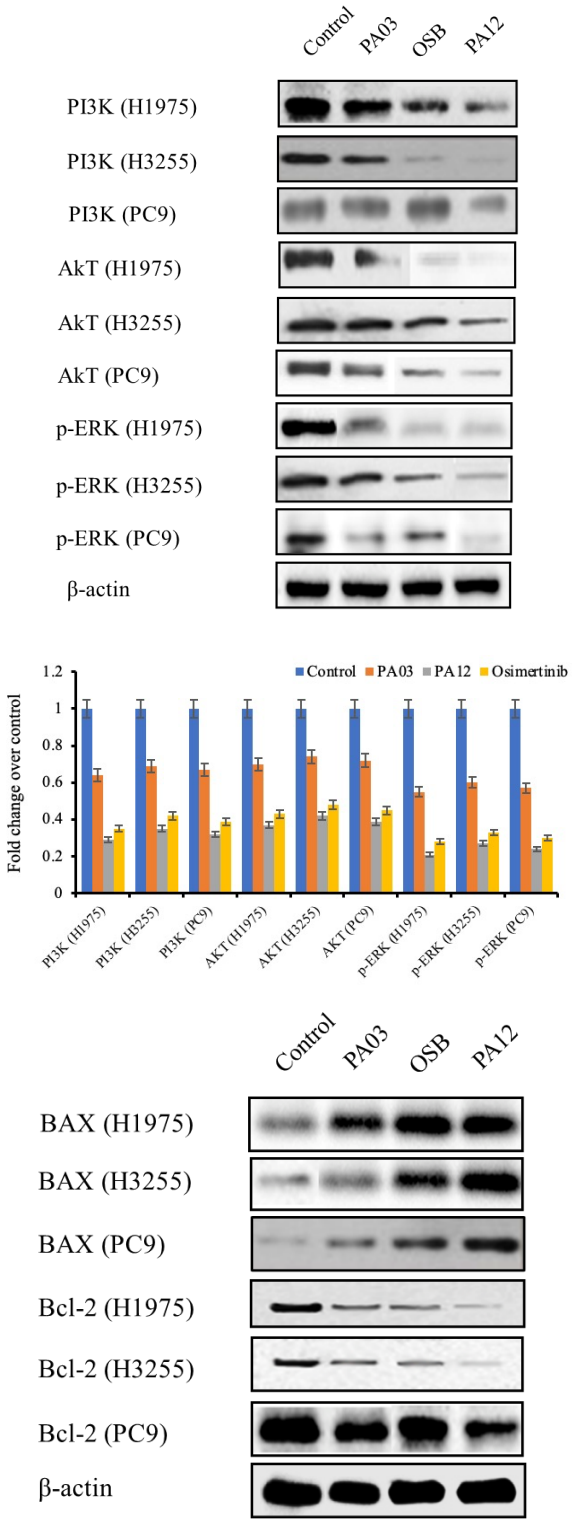

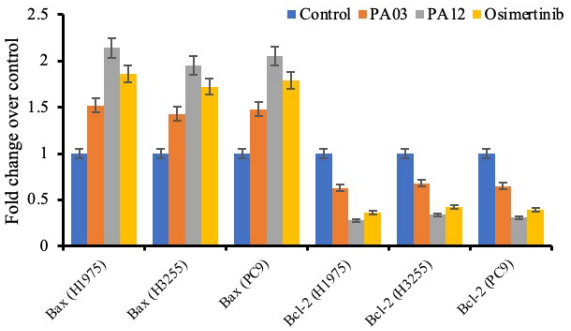

Figure 3. Western blot analysis of EGFR signaling, downstream pathways, and apoptosis following treatment with **PA03** and **PA12**; 3a. Representative Western blot images showing the expression of EGFR (A549), p-EGFR (A549), EGFR L858R (H1975, H3255), and EGFR T790M (H1975, PC9) following treatment with **PA03**, **PA12**, and osimertinib; 3b. Densitometric quantification of EGFR-related proteins expressed as fold change relative to control demonstrated significant suppression of mutant and phosphorylated EGFR by **PA12** compared to **PA03** and osimertinib (Figure 3c). Representative Western blot images depicting PI3K, AKT, and p-ERK expression in H1975, H3255, and PC9 cells, indicating modulation of downstream signaling pathways upon treatment for 3d. Quantitative analysis of PI3K/AKT/p-ERK signaling proteins, showing marked inhibition of pathway activation by **PA12** relative to **PA03** and the reference drug; 3e. Representative Western blot images of apoptotic markers Bax and Bcl-2 in H1975, H3255, and PC9 cells following treatment; 3f. Densitometric analysis of Bax and Bcl-2 expression levels, demonstrating enhanced pro-apoptotic signaling (Bax upregulation and Bcl-2 downregulation) with **PA12** treatment.Data are presented as mean ± SD (n = 3). Statistical significance was determined using one-way ANOVA followed by Tukey's post hoc test, with $p < 0.05$ considered statistically significant compared to control.

Caspase 3/7 and Caspase 9 assays

To further validate the pro-apoptotic potential of the optimized phosphoaspirin derivatives, caspase-3/7 and caspase-9 activities were quantified in NSCLC cell lines representing distinct EGFR mutational backgrounds. The results (Figure 4a and 4b) demonstrated a significant and concentration-dependent activation of both initiator and executioner caspases, confirming apoptosis induction as the key mechanism underlying the cytotoxic effects of **PA03** and **PA12**. As illustrated in Figure 4a, treatment with **PA12** resulted in the highest activation of caspase-3/7,

with fold increases of 2.76 ± 0.22 in H1975, 2.41 ± 0.19 in H3255, and 2.58 ± 0.21 in PC9 cells, compared to moderate activation by **PA03** (1.65–1.82 fold) and intermediate effects by osimertinib (2.08–2.34 fold). Notably, the magnitude of caspase-3/7 activation was relatively lower in A549 cells (2.05 ± 0.16), suggesting reduced sensitivity in wild-type EGFR. This pattern indicates a mutation-dependent enhancement of apoptosis, with the most pronounced effect observed in the dual mutant H1975 cells. Similarly, caspase-9 activity (Figure 4b) followed a consistent trend, with **PA12** inducing robust activation (2.52 ± 0.20 in H1975, 2.21 ± 0.18 in H3255, and 2.36 ± 0.19 in PC9), confirming the involvement of the intrinsic mitochondrial apoptotic pathway. In contrast, **PA03** exhibited comparatively lower activation (1.51–1.64 fold), whereas osimertinib demonstrated moderate induction (1.96–2.18 fold). The reduced activation observed in A549 cells (1.92 ± 0.15) further supports the mutation-selective apoptotic response of the cells. Importantly, the parallel increase in both caspase-9 and caspase-3/7 activities establishes a sequential apoptotic cascade, in which mitochondrial pathway activation (caspase-9) leads to downstream executioner caspase activation (caspase-3/7). These findings are in strong agreement with the western blot results showing Bax upregulation and Bcl-2 downregulation, thereby confirming mitochondrial membrane destabilization and cytochrome c-mediated apoptosis. Collectively, the caspase assay results demonstrated that **PA12** induced robust, mutation-selective apoptosis through the activation of the intrinsic pathway, with superior efficacy compared to **PA03** and comparable or enhanced activity relative to osimertinib. This mechanistic validation further reinforces the potential of **PA12** as a promising therapeutic candidate for targeting EGFR-driven NSCLC.

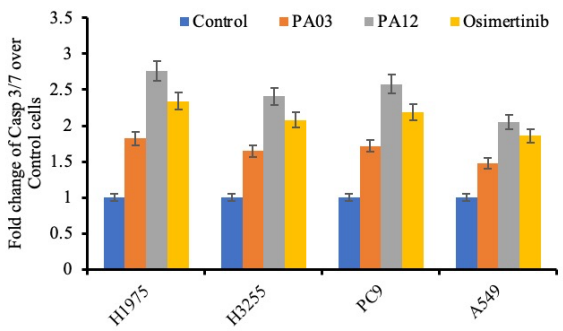

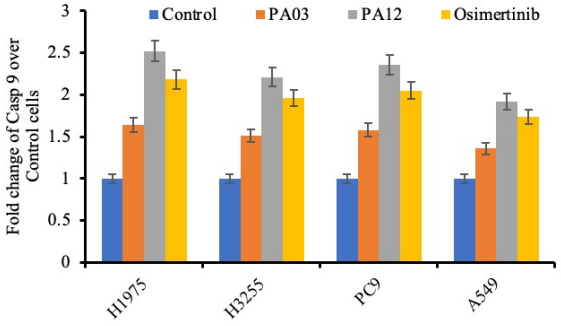

Figure 4. Caspase activation analysis following treatment with **PA03** and **PA12** in NSCLC cell lines. **4a:** Caspase-3/7 activity; **4b:** Caspase-9 activity expressed as fold change over control in H1975, H3255, PC9, and A549 cells after 24 h of treatment. **PA12** exhibited the highest activation of both executioner (caspase-3/7) and initiator (caspase-9) caspases across all cell lines, followed by osimertinib and **PA03** treatment. This effect was more pronounced in mutant cell lines (H1975 and PC9) than in wild-type A549 cells, indicating mutation-selective apoptosis induction. Data are presented as mean ± SD (n = 3). Statistical analysis was performed using one-way ANOVA followed by Tukey's post hoc test (*$p < 0.05$ vs. control).

In vivo antitumor evaluation in H1975 xenograft model

The in vivo therapeutic efficacy of the optimized phosphoaspirin derivative, PA12, was evaluated using an H1975 xenograft model representing clinically relevant EGFR L858R/T790M-resistant NSCLC. Tumor progression profiles (Figure 5a) demonstrated a time-dependent increase in tumor volume in the control group, reaching approximately 1350 mm³ by day 28, confirming aggressive tumor growth in the absence of treatment. In contrast, **PA12** treatment resulted in marked suppression of tumor progression, with final tumor volumes limited to approximately 520 mm³, indicating substantial antitumor activity. Notably, **PA12** exhibited superior efficacy compared to osimertinib, which showed a final tumor volume of approximately 610 mm³, highlighting the enhanced therapeutic potential of **PA12** in resistant tumor models. Quantitative analysis of excised tumors (Table 4) further supported these findings, where **PA12** significantly reduced tumor weight to 0.58 ± 0.05 g, corresponding to a tumor growth inhibition (TGI) of 61.8% compared to 55.3% for osimertinib. This improvement underscores the ability of **PA12** to effectively suppress tumor burden beyond the current standard-of-care EGFR inhibitor. Importantly, safety and tolerability assessments revealed no significant

adverse effects associated with **PA12** treatment in the present study. As shown in Figure 5b, the body weight remained stable throughout the treatment period, with no notable differences compared to the control and osimertinib groups, indicating the absence of systemic toxicity. Furthermore, serum biochemical parameters (Table 5), including AST, ALT, urea, and creatinine, remained within the normal physiological range, confirming the hepatic and renal safety of the treatment. Collectively, these in vivo findings demonstrate that **PA12** exerts potent antitumor activity with a favorable safety profile, effectively inhibiting tumor growth in EGFR T790M/L858R-driven NSCLC. The superior efficacy of **PA12** over osimertinib, coupled with its minimal toxicity, suggests its strong translational potential as a next-generation therapeutic candidate for overcoming resistance in NSCLC.

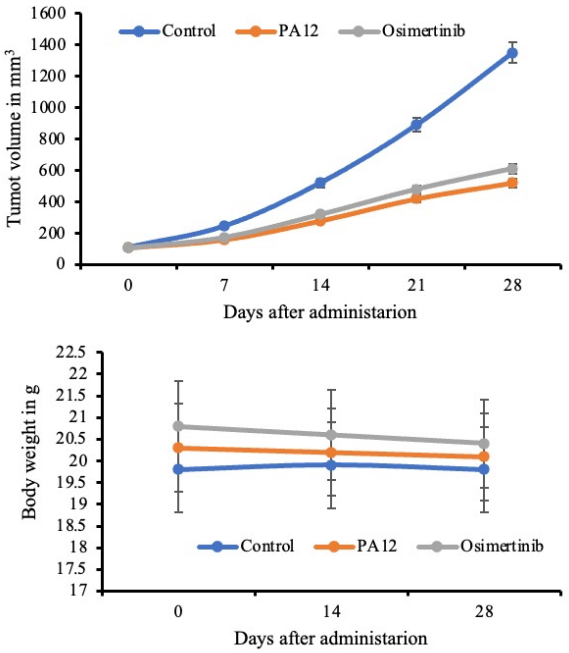

Figure 5. *In vivo* antitumor efficacy of **PA12** in H1975 xenograft model; **5a.** Top panel: Tumor growth curves showing a progressive increase in tumor volume over 28 days post-treatment. **PA12** treatment significantly suppressed tumor progression compared to the control and exhibited improved efficacy relative to osimertinib. **5b.** Body weight profiles indicated minimal variation across groups, suggesting good tolerability and the absence of systemic toxicity. **PA12**-treated animals maintained a stable body weight comparable to that of the control and osimertinib groups. Data are presented as mean ± SD (n = 6). Statistical analysis was performed using two-way ANOVA for tumor growth and one-way ANOVA for body weight, followed by Tukey's post-hoc test (*p < 0.05 vs. control).

Table 4. Final tumor weight and tumor growth inhibition (TGI%)

Group	Tumor weight (g)	TGI (%)
Control	1.52 ± 0.12	—
PA12	0.58 ± 0.05	61.8
Osimertinib	0.68 ± 0.06	55.3

Table 5. Serum biochemical parameters (safety assessment)

Parameter	Control	PA12	Osimertinib
AST (U/L)	48.5 ± 4.1	45.1 ± 3.6	47.8 ± 4.6
ALT (U/L)	42.3 ± 3.2	40.2 ± 3.7	42.7 ± 3.6
Urea (mg/dL)	28.7 ± 2.8	26.7 ± 2.2	27.3 ± 2.9
Creatinine (mg/dL)	0.78 ± 0.05	0.75 ± 0.04	0.77 ± 0.05

CONCLUSION

In summary, the present study demonstrates that the optimized phospho-aspirin derivative, PA12, exhibits potent and mutation-selective anticancer activity against EGFR T790M/L858R-driven resistant NSCLC. PA12 exhibited superior in vitro antiproliferative efficacy, favorable selectivity toward cancer cells, and strong inhibition of mutant EGFR kinase activity compared to PA03 and benchmark inhibitors. Mechanistic investigations confirmed the effective suppression of EGFR activation and downstream PI3K/AKT and MAPK/ERK signaling pathways, along with the robust induction of mitochondrial apoptosis, as evidenced by the modulation of Bax/Bcl-2 expression and the activation of caspase-9 and caspase-3/7. Importantly, in vivo validation in the H1975 xenograft model revealed significant tumor growth inhibition with PA12, exceeding the efficacy of osimertinib while maintaining a favorable safety profile without detectable systemic toxicity. Collectively, these findings establish PA12 as a promising next-generation EGFR-targeted therapeutic candidate with strong translational potential for overcoming NSCLC resistance. Further studies focusing on pharmacokinetics, long-term safety, and clinical validation are warranted.

Acknowledgements

The authors gratefully acknowledge the Indian Council of Medical Research (ICMR), Government of India, for funding this project (grant no. 3/2/2/42/2018/Online Onco Fship/NCD-III). The authors also thank Anurag University for providing the necessary technical facilities and support to successfully conduct this research.

Author Credits

Dr Vasudha Bakshi: Conceptualization, supervision, and guidance; Dr. Appaji Dokala: Conceptualization, Data Analysis, Manuscript Review; Mrs Madhuri Rudraraju: Investigation, Work execution, Writing-original draft, Writing- Review & Editing.

Funding

Non-available

Ethical statement

This article contains no studies with human participants or animals performed by the authors.

Conflict of interest

The authors declare that they have no competing financial interests or personal relationships that might have influenced their work.

REFERENCES

Brentnall, M., Rodriguez-Menocal, L., De Guevara, R.L., Cepero, E., Boise, L.H. (2013). Caspase-9, caspase-3 and caspase-7 have distinct roles during intrinsic apoptosis. *BMC Cell Biology*, 14, 32.

Cross, D.A., Ashton, S.E., Ghiorghiu, S., Eberlein, C., Nebhan, C.A., Spitzler, P.J., Orme, J.P., Finlay, M.R.V., Ward, R.A., Mellor, M.J., Hughes, G., Rahi, A., Jacobs, V.N., Red Brewer, M., Ichihara, E., Sun, J., Jin, H., Ballard, P., Al-Kadhimi, K., Rowlinson, R., Klinowska, T., Richmond, G.H., Cantarini, M., Kim, D.W., Ranson, M.R., Pao, W. (2014). AZD9291, an irreversible EGFR TKI, overcomes T790M-mediated resistance. *Cancer Discovery*, 4, 1046–1061.

Cuzick, J., Thorat, M.A., Bosetti, C., Brown, P.H., Burn, J., Cook, N.R., Ford, L.G., Jacobs, E.J., Jankowski, J.A., La Vecchia, C., Law, M., Meyskens, F., Rothwell, P.M., Senn, H.J., Umar, A. (2015). Aspirin and non-steroidal anti-inflammatory drugs for cancer prevention. *The Lancet Oncology*, 16, e565–e575.

Herbst, R.S., Morgensztern, D., Boshoff, C. (2018). Lung cancer. *New England Journal of Medicine*, 378, 207–220.

Hua, H., Zhang, H., Chen, J., Wang, J., Liu, J., Jiang, Y. (2020). Phospho-aspirin derivatives as anticancer agents. *Cancer Letters*, 475, 1–10.

Jänne, P.A., Yang, J.C.H., Kim, D.W., Planchard, D., Ohe, Y., Ramalingam, S.S., Ahn, M.J., Kim, S.W., Su, W.C., Horn, L., Haggstrom, D., Felip, E., Kim, J.H., Frewer, P., Cantarini, M., Brown, K.H., Dickinson, P.A., Ghiorghiu, S., Ranson, M. (2015). AZD9291 in EGFR inhibitor-resistant NSCLC. *New England Journal of Medicine*, 372, 1689–1699.

Leonetti, A., Sharma, S., Minari, R., Perego, P., Giovannetti, E., Tiseo, M. (2019). Resistance mechanisms to osimertinib in EGFR-mutated non-small cell lung cancer. *British Journal of Cancer*, 121, 725–737.

Mok, T.S., Wu, Y.L., Thongprasert, S., Yang, C.H., Chu, D.T., Saijo, N., Sunpaweravong, P., Han, B., Margono, B., Ichinose, Y., Nishiwaki, Y., Ohe, Y., Yang, J.J., Chewaskulyong, B., Jiang, H., Duffield, E.L., Watkins, C.L., Armour, A.A., Fukuoka, M. (2009). Gefitinib or chemotherapy for EGFR-mutated NSCLC. *New England Journal of Medicine*, 361, 947–957.

Mosmann, T. (1983). Rapid colorimetric assay for cellular growth and survival: Application to proliferation and cytotoxicity assays. *Journal of Immunological Methods*, 65, 55–63. https://doi.org/10.1016/0022-1759(83)90303-4

Pao, W., Miller, V., Zakowski, M., Doherty, J., Politi, K., Sarkaria, I., Singh, B., Heelan, R., Rusch, V., Fulton, L., Mardis, E., Kupfer, D., Wilson, R., Kris, M., Varmus, H. (2005). Acquired resistance of lung adenocarcinomas to gefitinib or erlotinib. *PLoS Medicine*, 2, e73.

Promega Corporation (2024). ADP-Glo™ Kinase Assay Technical Manual. Promega Corporation.

Pushpakom, S., Iorio, F., Eyers, P.A., Escott, K.J., Hopper, S., Wells, A., Doig, A., Guilliams, T., Latimer, J., McNamee, C., Norris, A., Sanseau, P., Cavalla, D., Pirmohamed, M. (2019). Drug repurposing: Progress, challenges and recommendations. *Nature Reviews Drug Discovery*, 18, 41–58.

Rudraraju, M., Dokala, A., Bakshi, V. (2022). Design, synthesis and in vitro evaluation of novel phospho-aspirin derivatives as potent inhibitors of EGFR T790M/L858R mutants in EGFR–

HER2 driven NSCLC cancer: A drug repurposing strategy. *European Chemical Bulletin*, 11, 1010–1029.

Santarpia, M., Liguori, A., Karachaliou, N., Gonzalez-Cao, M., Daffinà, M.G., D'Aveni, A., Marabello, G., Altavilla, G., Rosell, R. (2017). Osimertinib in the treatment of NSCLC: Design and clinical application. *Lung Cancer: Targets and Therapy*, 8, 109–125.

Sequist, L.V., Yang, J.C.H., Yamamoto, N., O'Byrne, K., Hirsh, V., Mok, T., Geater, S.L., Orlov, S., Tsai, C.M., Boyer, M., Su, W.C., Bennouna, J., Kato, T., Gorbunova, V., Lee, K.H., Shah, R., Massey, D., Zazulina, V., Shahidi, M., Schuler, M. (2013). Afatinib versus chemotherapy for EGFR-mutant NSCLC. *Journal of Clinical Oncology*, 31, 3327–3334.

Sharma, S.V., Bell, D.W., Settleman, J., Haber, D.A. (2007). Epidermal growth factor receptor mutations in lung cancer. *Nature Reviews Cancer*, 7, 169–181.

Siegel, R.L., Miller, K.D., Wagle, N.S., Jemal, A. (2023). Cancer statistics. *CA: A Cancer Journal for Clinicians*, 73, 17–48.

Soria, J.C., Ohe, Y., Vansteenkiste, J., Reungwetwattana, T., Chewaskulyong, B., Lee, K.H., Dechaphunkul, A., Imamura, F., Nogami, N., Kurata, T., Okamoto, I., Zhou, C., Cho, B.C., Cheng, Y., Cho, E.K., Voon, P.J., Planchard, D., Su, W.C., Gray, J.E., Lee, S.M., Hodge, R., Marotti, M., Rukazenkov, Y., Ramalingam, S.S. (2018). Osimertinib in untreated EGFR-mutated advanced NSCLC. *New England Journal of Medicine*, 378, 113–125.

Yarden, Y., Sliwkowski, M.X. (2001). Untangling the ErbB signaling network. *Nature Reviews Molecular Cell Biology*, 2, 127–137.

Yun, C.H., Boggon, T.J., Li, Y., Woo, M.S., Greulich, H., Meyerson, M., Eck, M.J. (2008). Structures of lung cancer-derived EGFR mutants and inhibitor complexes. *Proceedings of the National Academy of Sciences USA*, 105, 2070–2075.

Zegzouti, H., Zdanovskaia, M., Hsiao, K., Goueli, S.A. (2009). ADP-Glo: A bioluminescent and homogeneous ADP monitoring assay for kinases. *Assay and Drug Development Technologies*, 7, 560–572.

Zhang, T., Qu, R., Chan, S., Chen, J., Wang, Y., Wang, J. (2020). Discovery of a novel third-generation EGFR inhibitor and its activity in EGFR-mutant models. *Cancer Biology & Medicine*, 17, 1–14.

Zhao, W., Luo, J., Wang, Y., Liu, Y., Wang, J., Sun, Y. (2018). Phospho-aspirin derivatives in cancer therapy. *Oncotarget*, 9, 345–357.